Design Limitations of Highly Parallel Free-Space Optical Interconnects Based on Arrays of Vertical Cavity Surface-Emitting Laser Diodes, Microlenses, and Photodetectors

Suning Tang, Ray T. Chen, *Member, IEEE,* Lara Garrett, Dave Gerold, and Maggie M. Li

Abstract—**We utilize a novel diffraction formalism to study the crosstalk effect in a highly parallel free-space optical interconnect based on two-dimensional arrays of surface-emitting laser diodes, microlenses, and photodetectors. The diffraction induced crosstalk between adjacent laser diodes in each detector to the system limitations is investigated. Optimum design rules and formulas are given for the first time, to include the relation of channel packaging density and interconnect length to the design parameters of the optical interconnect components. The design formulas developed here yield an optimum detector size and indicate a tradeoff between channel packaging density and interconnect length. The feasibility of such a free-space interconnect with a channel packaging density of 3460 channels/cm^2 and 2.0 cm interconnection length is determined using typical parameters of detector radius from ~5 to ~45 μm, lens radius of 85 μm, and laser diode radius of ~5 μm operating at wavelength 0.67 μm for signal-to-noise ratio above 12 dB. Some experiments were conducted to measure the diffraction induced crosstalk and optical link efficiency.**

TECHNICAL advancements in microfabrication have permitted electronic devices to be packed ever more densely, producing a consequent increase in the number of signal paths needed for device interconnection. This, combined with constantly increasing demand for signal speed, has resulted in problems of signal skew and bandwidth limitation of electrical interconnects. Free-space optical interconnects are of increasing interest as a replacement for electrical interconnects in high performance digital computers [1]–[4]. Very recently, a new type of free-space optical interconnect, based on the feasibility of integrating a microlens array with a surface-emitting laser diode array and a photodetector array, was proposed along with preliminary demonstrations [5]–[8]. A number of advantages are associated with such an optical interconnect architecture. These include high link efficiency, massive parallelism, wide bandwidth, and high speed. More important, because all of the "microbeams" propagate at the same angle, the difficulties associated with the multiple individual alignment in three spatial and three angular coordinates with very narrow tolerance are not longer present [8].

As one of the key parameters of an optical interconnect network, the packing density (number of pixels/cm^2) has been investigated for various optical interconnect networks [9]–[12]. Analytic techniques used include an application of Gabor's theory in a free-space interconnect [13], a multiple-scattering model in volume holographic interconnections [14], and a crosstalk model relating the cross-coupling among 2-D channel waveguides [15], [16]. Ray-tracing and Gaussian beam estimations were used to study the device performance in terms of optical loss in the previously reported highly parallel free-space optical interconnect networks based on arrays of vertical cavity surface-emitting lasers (VCSEL's) and microlenses [5]–[8]. In these estimations, the effects of diffraction from the apertures of the microlenses on the system size and performance have not been extensively explored. Such diffraction effects are significant since their presence introduces power loss, crosstalk, and coherent artifact noise. The further study of such diffraction effects can greatly impact the understanding of the device capability and improve future device performance.

In this paper, a crosstalk model, to include diffraction induced cross-coupling among pixels, is developed to study packing density of the massively parallel free-space point-to-point optical interconnect network shown in Fig. 1. The presented interconnect network utilizes arrays of VCSEL's, microlenses, and photodetectors, capable for future integration [see Fig. 1(b)]. Based on the crosstalk model, variations of packing density and optical transmission efficiency were investigated for the first time, in terms of diffraction induced crosstalk. To verify the theory presented, experiments were conducted to measure the optical link efficiency and diffraction induced crosstalk. Optimum design criteria for the radii of laser output window, microlens, and photodetector were further delineated for the first time.

The schematic setup representing the point-to-point optical interconnect network under consideration is shown in Fig. 1. We assume the presence of an array of vertical cavity surface-emitting laser diodes with output window radius a, followed by an array of microlenses with lens radius ω_o and focal length f. An array of photodetectors with detector radius a_d is located at the receiving plane. The laser-to-laser and detector-to-detector

Manuscript received September 7, 1993; revised July 19, 1994. This work was supported by Cray Research, Inc., ARPA, Novex Corporation, Physical Optics Corporation, Army Research Office, and the University of Texas at Austin.

The authors are with the Microelectronics Research Center, Department of Electrical and Computer Engineering, University of Texas, Austin, TX 78712-1084.

IEEE Log Number 9405771.

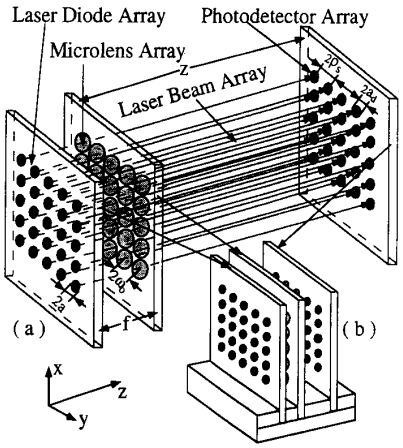

Fig. 1. (a) A schematic diagram of a highly parallel free-space optical interconnect based on arrays of surface-emitting laser diodes, microlenses, and photodetectors. (b) An integrated diagram.

separation are 2ρ. The microlens array, located at a diode-lens distance equal to the lens focal length, is utilized to collimate the output beams from the VCSEL array on to a photodetector array [5]–[8]. The separation distance z between microlens array and photodetector array is defined as the interconnection length. Based on Gabor's theory of information, circular symmetry of the optical elements (laser diodes, lenses, and detectors), corresponding to highest degree of symmetry is preferred and thus selected in the following discussion to increase the interconnect fidelity [13]. The arranging lattice of the two-dimensional array (see Fig. 1) is selected in square-packed pattern, which has been used by previous researchers [3], [5], [6], [8].

The optical wave emitted from the vertical cavity surface-emitting laser diode can be assumed to be a plane wave diffracted by an output window of finite extent [17]. Accepting the validity of Fraunhofer approximation [18], i.e., $a^2/2\lambda \ll f$, the normalized amplitude of the electrical field distribution $E(\omega)$ at the plane of microlens array is simply the Fourier–Bessel transform of $E(r)$, evaluated at spatial frequency of $\omega/\lambda f$, given by

$$E(\omega) = \boldsymbol{B}\{E(r)\} = \frac{J_1(ka\omega/f)}{(ka\omega/f)} \tag{1}$$

and

$$E(r) = \text{circ}\left(\frac{r}{a}\right) = \begin{cases} 1 & (r \le a) \\ 0 & (\text{otherwise}). \end{cases} \tag{2}$$

$\boldsymbol{B}$ stands for the Fourier–Bessel transformation; circ (r/a) accounts for the finite extent of laser output window with radius of a; J_1 is the first-order Bessel function of the first kind; r and ω are the radii in polar coordinates in the plane of laser output window and the plane of microlens, respectively; $k = 2\pi/\lambda$ is the wave vector in free-space; and λ is optical operating wavelength (see Fig. 1). Denoting $P(\omega_o)$ as the fraction of the total normalized power contained within the circular aperture of lens with radius of ω_o at the plane of lens array (see Fig. 1), we have

$$P(\omega_o) = 2\pi \int_o^{\omega_o} [E(\omega)]^2 \omega \, d\omega = 1 - [J_0(ka\omega_o/f)]^2 - [J_1(ka\omega_o/f)]^2 \tag{3}$$

where J_0 is the fundamental order Bessel function of the first kind. $(1 - P(\omega_o))$ represents the total energy not collected by the microlens.

In the optical interconnect network shown in Fig. 1, a fraction of the uncollected energy $(1 - P(\omega_o))$ may transmit to other detectors through neighboring lenses. We assume that the overlap of the lens aperture and radial fields from other lasers contributes to crosstalk noise. This part of crosstalk noise thus can be approximated by

$$P_{n1} = P'_{n1} + P''_{n1} = 4\left\{ \int_{\omega_o}^{3\omega_o} \int_{\theta_1}^{\theta_2} [E(\omega)]^2 \omega \, d\omega \, d\theta + \int_{\omega_1}^{(\omega_1 + 2\omega_o)} \int_{\theta_3}^{\theta_4} [E(\omega)]^2 \omega \, d\omega \, d\theta \right\} \tag{4}$$

where P'_{n1} and P''_{n1} stand for the diffraction noises from nearest lasers and second nearest lasers collected by a detector, R is the ratio of detector diameter to the separation between two adjacent detectors, and $\omega_1 = (2\sqrt{2} - 1)\omega_o$. $\theta_1 - \theta_2$ and $\theta_3 - \theta_4$ are the angles covered by the nearest lens and second nearest lens in polar coordinates, respectively.

To determine the system limitation, the diffraction of the microlens array employed has to be considered as well. Because the surface-emitting laser diode is placed at the front focal point of the lens, the output electric field from a lens can be described as a quasi-plane wave with a finite aperture of ω_o, i.e.,

$$E(\omega) = E(\omega) \, \text{circ}\left(\frac{\omega}{\omega_o}\right) \tag{5}$$

where the electrical field $E(\omega)$ incident on a corresponding microlens is given by (1), the circle function accounts the finite extent of the lens aperture of radius ω_o. To find the distribution $E(\rho)$ of the field amplitude across the plane of the photodetector array, the Huygens–Fresnel principle [17] is applied to obtain

$$E(\rho) = \int\int_{\Sigma_i} \frac{\exp(jkl)}{j\lambda l} \cos(\boldsymbol{n}, \boldsymbol{l}) E(\omega) \, d\omega \, d\theta_i \tag{6}$$

where $l = (z^2 + \rho^2)^{0.5}$ and ρ is the radius in polar coordinates at the photodetector plane. $\boldsymbol{n}$ is the normal vector to the plane of microlens. θ_i are the angles covered by lens apertures of Σ_i. The total power of the optical signal collected by a detector with radius a_d, given as

$$P_s(a_d) = 2\pi \int_o^{a_d} [E(\rho)]^2 \rho \, d\rho \approx P(\omega_o)\{1 - [J_0(k\omega_o a_d/z)]^2 - [J_1(k\omega_o a_d/z)]^2\}. \tag{7}$$

$P(\omega_o)$ is the optical power given by (3). We assume that the overlap of the detector aperture and radial fields from other lasers through other microlens also contributes to crosstalk noise. The total power of the crosstalk noise P_{n2} due to lens diffraction and collected by each detector placed at distance z from the lens array plane is derived as

$$P_{n2} = P'_{n2} + P''_{n2} = 4\left\{\int_{2\rho_s - a_d}^{2\rho_s + a_d}\int_{\theta_6}^{\theta_5} |E(\rho)|^2 \rho\, d\rho\, d\theta + \int_{2\rho'_s - a_d}^{2\rho'_s + a_d}\int_{\theta_8}^{\theta_7} |E(\rho)|^2 \rho\, d\rho\, d\theta\right\} \quad (8)$$

where P'_{n2} and P''_{n2} stand for diffraction noises from the nearest lenses and the second nearest lenses. Here, $\theta_6 - \theta_5$ and $\theta_8 - \theta_7$ (shown in Fig. 3) are the angles covered by the detector in reference to the center of the nearest and the second nearest detectors in the detector plane. $2\rho_s$ is the minimum detector-to-detector separation satisfying the desired S/N ratio criterion and $\rho'_s = \sqrt{2}\rho_s$. Obviously, we should select $\omega_o = \rho_s$ in an optimum design.

The total power of the optical signal collected by a detector is given by (7), while the total optical diffraction noise is the sum of P_{n1} and P_{n2}, given by (4) and (8), respectively. Equations (4), (7), and (8) are key formulas for studying the free-space optical point-to-point interconnect network shown in Fig. 1. Based on (4), (7), and (8), the signal-to-noise ratio (SNR) can be obtained as a function of system design parameters, such as operating wavelength, detector-lens separation, detector-detector separation, lens focal length, the radius of laser output window, microlens, and photodetector. Optimum designs can be obtained through computer simulation, in order to maximize the system capabilities for a desired SNR. The tradeoff between channel packaging density and interconnection length can also be studied. It should be noted that the effects of microlens aberration, nonuniformity, and optical scattering and reflection were not included in our analysis, which are also important factors in system design and performance. In the case when the laser beam from each diode is coherent, constructive interference and artifact noise (optical coherent beating noise) may occur and result in an increased crosstalk noise in a detector. Because the optical constructive interference and coherent beating are strongly dependent on the phase, polarization, spectral linewidth of the lasers, and the electrical bandwidth of photodetector, a detailed derivation to predict the locations of the ghost spot and power of the crosstalk noise associated is beyond the scope of this paper and perhaps not available at this time.

To find the design limitations and optimum design rules, we specify a desired SNR, $N(\text{dB}) = 10\log_{10} P_s/P_n$. In a high-speed digital transmission system, the SNR must be large enough to ensure the required bit-error-rate [12], [13]. For example, 12 dB SNR is needed to ensure a bit-error-bit of 10^{-15} at a transmission rate of 500 MHz [12], which is equivalent to the clock speed of CRAY GaAs ECL machine.

Fig. 2 plots SNR versus detector-lens radius ratio with lens radius as a para meter (ω_o =85 and 100 μm) based on (4), (7), and (8). In the simulation, the typical values $a = 5$ μm;

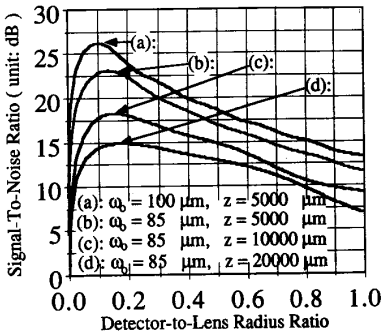

Fig. 2. The signal-to-noise ratio versus detector-to-lens radius ratio with the lens radius and interconnection length as parameters based on (4), (7), and (8).

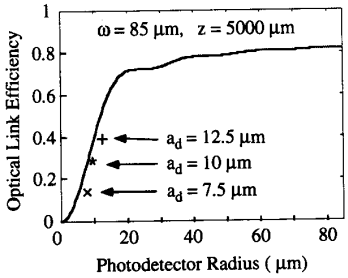

Fig. 3. Measured and theoretical optical link efficiency versus photodetector radius based on (7).

$\lambda = 0.67$ μm; $f = 425$ μm; and $z = 5000, 10\,000$, and $20\,000$ μm were assigned. The SNR drops very rapidly when detector size decreases, as shown in Fig. 2. The optimum detector size ranges from 10 to 15 μm in radius. As indicated by curve (d) in Fig. 2, the SNR is above 12 dB at the lens radius above 85 μm and detector radius from 5 to 45 μm. These are the standard sizes for commercial microlens and high-speed (> 1 GHz) photodetector, corresponding to a channel packaging density of 3460 channels/cm^2 at an interconnect length of 2.0 cm. For same device parameters [curves (b), (c), and (d)], the SNR drops slowly with increasing interconnection length for large detector size. This implies that only two-dimensional optical/mechanical alignment is required to construct the optical interconnect shown in Fig. 1.

The optical link efficiency is strongly dependent on the photodetector size. Fig. 3 shows the optical link efficiency versus photodetector size based on (7), where $\lambda = 0.67$ μm, $a = 5$ μm, $f = 425$ μm, $\omega_o = 85$ μM, and $z = 5000$ μm were assumed. (8% reflection loss was assumed in plotting Fig. 3 based on (7).) In such free-space optical interconnect systems, no external laser driver, detector preamplifier, or other interface circuitry was required at a transmitting rate of 1 GHz because of the high efficiency of the link [2].

In order to verify the formula developed herein, the optical link efficiency is measured at 0.5 cm interconnection length. The results were plotted in Fig. 3 against the theoretical plot based on (7). In the experiment, the VCSEL was simulated by a collimated Toshiba laser diode ($\lambda = 0.67$ μm) through a small pinhole with aperture 10 μm. The optical power

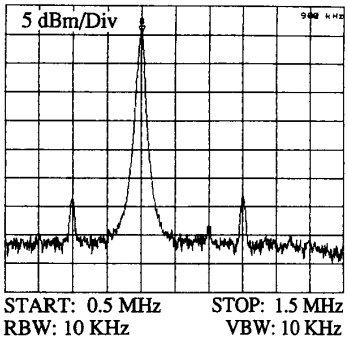

Fig. 4. Measured optical signal and crosstalk from two side channels at $z = 0.5$ cm.

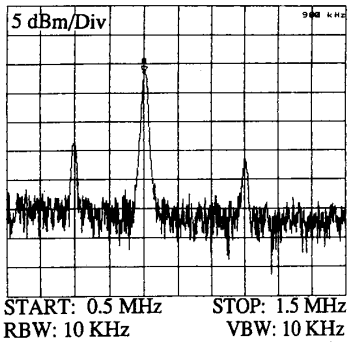

Fig. 5. Measured optical signal and crosstalk from two side channels at $z = 2.0$ cm.

right after the pinhole is measured and adjusted to 200 μW. The microlens was positioned carefully with the pinhole near its focal plane so that the transmitting laser beam was approximately collimated. The microlens (array) employed has a radius of 85 μm, lens-to-lens separation of 200 μm, and a focal length of 425 μm. The optical power for detecting the link efficiency was measured by Newport Optical Power Meter (Model 818J25) through an aperture, carefully aligned along the laser beam and located 0.5 cm away from microlens. Three apertures with radius of 15, 20, and 25 μm were employed in the measurements, respectively, mimicking three different detector sizes. All pinholes and microlens (array) were mounted on the 3-dimensional microtranslation stage, respectively, with a resolution of ± 1 μm. Fig. 3 shows the reasonable agreement between experimental results and theoretical plot based on (7).

To demonstrate and determine the optical crosstalk among each channel, the input laser was further amplitude modulated at three different frequencies (0.9, 0.7, and 1.1 MHz), respectively, representing signal from three different lasers. The modulated laser beam transmitting through the microlens array was again detected by the power meter through a 7.5 μm radius pinhole located 0.5 cm away from microlens array. The modulated signal was measured three times by aligning the pinhole (7.5 μm) with its own lens and with its two nearest neighboring lenses, respectively, corresponding to the frequency component of 0.9, 0.7, and 1.1 MHz in RF spectrum. Three different modulation frequencies were used to allow display crosstalk and signal on the same display screen. The measured results were recorded by an RF Spectrum Analyzer (Model HP 8566B) three times each, and added together shown in Fig. 4. Each time, the power of the modulated laser beam was adjusted at the same level ($\sim$200 μW), monitored at the center channel. The channel crosstalk was successfully determined at a SNR of $\sim$ 28 dB shown in Fig. 4. The SNR drops to $\sim$ 15 dB at the interconnection length of $\sim$ 2.0 cm in the experiment as shown in Fig. 5. Note that these SNR's are better than the 12 dB requirement adopted.

Free-space point-to-point optical interconnects employing arrays of VCSEL's, microlenses, and photodetectors were analyzed based on the diffraction induced crosstalk model developed herein. Limitations on packing density and interconnection length due to diffraction induced crosstalk were investigated. System performance in terms of S/N ratio was simulated as device parameters of the arrays of VCSEL's, microlenses, and photodetectors. The channel packing density of 3460 pixels/cm^2 with interconnection length 2.0 cm was determined by the simulations based on both theory and experiment, through employing typical commercial device parameters. Free-space massively parallel point-to-point interconnects are very promising compared to guided wave interconnects, where earlier results shows packing density of 750 channel/cm with interconnection length 2.0 cm in a 2-dimensional single-mode channel waveguide array [16]. An important result is that the interconnect presented herein requires little surface real estate in the receiver plane, which may be intensively occupied by existing electronic components such as VLSI multichip modules. Such a highly parallel free-space optical interconnect system is suitable for massively parallel processing systems such as board-to-board and module-to-module interconnects [4]–[8], [20], [21].

REFERENCES

[1] J. W. Goodman, F. J. Leonberger, S.-Y. Kung, and R. A. Athale, "Optical interconnections for VLSI systems," *Proc. IEEE,* vol. 72, pp. 850–866, 1984.
[2] D. Z. Tsang, "High-speed optical interconnections for digital systems," *Lincoln Lab. J.*, vol. 4, no. 1, pp. 31–44, 1991.
[3] H. S. Hinton, "Progress in systems based on free-space interconnection," *SPIE,* vol. 1849, pp. 2–3, 1993.
[4] R. T. Chen, H. Lu, D. Robinson, Z. Sun, and T. Jannson, D. V. Plant, and H. R. Fetterman, "60 GHz board-to-board optical interconnection using polymer optical buses in conjunction with microprism couplers," *Appl. Phy. Lett.*, vol. 60, pp. 536–538, 1992.
[5] S. Kawai, "Free-space multistage interconnection networks using microlens arrays," *J. Lightwave Technol.*, vol. 9, pp. 1774–1779, 1991.
[6] N. C. Craft and A. Y. Feldblum, "Optical interconnects based on arrays of surface-emitting lasers and lenslets," *Appl. Opt.*, vol. 31, pp. 1735–1739, 1992.
[7] R. P. Bryan, J. L. Jewell, G. R. Olbright, and W. S. Fu, "Smart pixel optoelectronics interconnects: Integrated microlasers-transistors," *SPIE,* vol. 1849, pp. 260–271, 1993.
[8] F. B. McCormick, F. A. P. Tooley, J. L. Brubaker, T. J. Cloonan, J. M. Sasian, H. S. Hinton, K. O. Mersereau, and A. Y. Feldblum, "Optical interconnections using microlens arrays," *Opt. Quantum Electron.*, vol. 24, pp. S465–S477, 1992.
[9] R. Barakat and J. Reif, "Lower bounds on the computational efficiency of optical computing systems," *Appl. Opt.*, vol. 26, pp. 1015–1018, 1987.
[10] M. R. Feldman and C. G. Guest, "Interconnect density capabilities of computer generated holograms for optical interconnection of very large scale integrated circuits," *Appl. Opt.*, vol. 28, pp. 3134–3137, 1989.

[11] M. R. Feldman, C. G. Guest, T. J. Drabik, and S. C. Esener, "Comparison between electrical and free space optical interconnects for fine grain processor arrays based on interconnect density capabilities," *Appl. Opt.*, vol. 28, pp. 3820–2829, 1989.
[12] J. W. Goodman, "Linear space-variant optical data processing," in *Optical Information Processing*, S. H. Lee, Ed. Berlin: Springer-Verlag, 1981, p. 248.
[13] N. Davidson, A. A. Friesem, and E. Hasman, "On the limits of optical interconnects," *Appl. Opt.*, vol. 31, pp. 5426–5430, 1992.
[14] K.-Y. Tu, H. Lee, and T. Tamir, "Analysis of cross talk in volume holographic interconnects," *Appl. Opt.*, vol. 31, pp. 1717–1729, 1992.
[15] C.-S. Li, C. M. Olsen, and D. G. Messerschmitt, "Analysis of crosstalk penalty in dense optical chip interconnects using single-mode waveguides," *J. Lightwave Technol.*, vol. 9, pp. 1693–1701, 1991.
[16] S. Tang, R. T. Chen, and M. Peskin, "Packing density and interconnect length limitations of a highly parallel optical interconnect using polymer-based single-mode bus array," *Opt. Eng.*, Special issue on Optical Interconnect and Packaging, pp. 1–6, May 1994.
[17] C. A. Evans, D. P. Bour, N. W. Carlson, R. Amantea, and J. M. Hammer *et al.*, "Characteristics of coherent two-dimensional grating surface emitting diode laser arrays during CW operation," *IEEE J. Quantum Electron.*, vol. 27, pp. 1594–1608, 1991.
[18] J. W. Goodman, *Introduction to Fourier Optics*. New York: McGraw-Hill, 1968, p. 61.
[19] R. P. MacDonald, J. Chrostowski, S. A. Boothroyd, and B. A. Syrett, "Holographic formation of a diode laser nondiffracting beam," *Appl. Opt.*, vol. 32, pp. 6470–6474, 1993.
[20] B. Robertson, E. J. Restall, M. R. Taghizadeh, and A. C. Walker, "Space-variant holographic optical elements in dichromated gelatin," *Appl. Opt.*, vol. 30, pp. 2368–2374, 1991.
[21] R. K. Kostuk, J.-H. Yeh, and M. Fink, "Distributed optical data bus for board-level interconnects," *Appl. Opt.*, vol. 32, pp. 5010–5020, 1993.

Suning Tang, photograph and biography not available at the time of publication.

Ray T. Chen (M'91) is currently with the Microelectronics Research Center of the Department of Electrical and Computer Engineering, University of Texas, Austin. He joined the university from the Department of Electrooptic Engineering of Physical Optics Corporation where he served as the department director from 1989 to 1992. Within the past six years he has been the author and the principal investigator for over thirty awarded research proposals sponsored by many subdivisions of DOD, NSF, DOE, NASA and other private industries such as Cray Research, Inc., Boeing, Physical Optics Corporation, Radiant Research, etc. His research is focused on polymer-based photonic integrated circuits for various military and civilian applications.

Dr. Chen has served as the chairman and a program committee member for over fifteen domestic and international conferences. He has also served as a consultant for photonic industry and federal government. He has over one hundred and thirty publications in open literature and delivered numerous invited talks in the professional societies. He is an active member of IEEE, SPIE, OSA, and PSC.

Lara Garrett, photograph and biography not available at the time of publication.

Dave Gerold, photograph and biography not available at the time of publication.

Maggie M. Li, photograph and biography not available at the time of publication.